Inorg. Chem. **2007**, *46*, 6565–6574

Structural and Mechanistic Studies of Bis(phenolato)amine Zinc(II) Catalysts for the Polymerization of ϵ-Caprolactone

Carter M. Silvernail, Letitia J. Yao, Lyndal M. R. Hill, Marc A. Hillmyer,* and William B. Tolman*

Department of Chemistry, University of Minnesota, 207 Pleasant St. SE, Minneapolis, Minnesota 55455

Received March 27, 2007

The syntheses, characterization, ϵ-caprolactone (CL) polymerization activity, and kinetics investigation of two zinc(II) bis(phenolato)amine complexes L_2Zn_2 are reported (L = methylamino-*N*,*N*-bis(2-methylene-4,6-di-*tert*-butylphenolato) and/or methylamino-*N*,*N*-bis(2-methylene-4-adamantyl-6-*tert*-butylphenolato)). X-ray crystallographic and ^{1}H NMR studies, including NOESY and PGSE experiments, provided insight into the solid and solution state structures, respectively, as well as evidence for the catalytically active species responsible for the ring-opening polymerization of CL. Additionally, solution polymerizations and kinetic experiments involving $(L^1)_2Zn_2$ in the presence of benzyl alcohol (BnOH) were performed to elucidate the influence of catalyst structure, solvent, and the concentration dependence of the catalytically active species, CL, and BnOH on the rate and control of poly-ϵ-caprolactone (PCL) formation. The structural, polymerization, and kinetic data support equilibria involving both mononuclear and dinuclear forms of $(L^1)_2Zn_2$ as well as a monomer-activated route to PCL.

Introduction

Polyesters derived from renewable resources have attracted considerable attention over the last two decades as biocompatible and biodegradable alternatives to petrochemically derived plastics. In particular, the aliphatic polyester polylactide (PLA) has found global applications for many biomedical and pharmaceutical applications including medical implants, sutures, and drug delivery devices.[1] PLA and other aliphatic polyesters are traditionally prepared via ring-opening polymerization (ROP) of cyclic esters through a coordination-insertion pathway involving a metal alkoxide catalyst (Scheme 1, top).[2] This route has provided both rapid and stereoselective conversion to the desired polyesters with exceptional molecular weight control and narrow polydispersities. Furthermore, kinetic studies have provided detailed mechanistic information pertaining to this pathway,[3] including insight into effects of ligand and metal variation on polymerization activity.[4]

Alternatively, an activated monomer pathway (Scheme 1, bottom) has also been proposed for the ROP of cyclic esters. This route has been suggested for the ROP of lactones with protic acid/alcohol combinations that result in low molecular weight polyesters with broad molecular weight distributions.[5] More recently, nucleophilic organocatalysts in conjunction with alcohol initiators have been shown to exhibit remarkable activity for the polymerizations of cyclic esters under mild

* To whom correspondence should be addressed. E-mail: hillmyer@chem.umn.edu (M.A.H.), tolman@chem.umn.edu (W.B.T.).

(1) (a) Coulembiera, O.; Degée, P.; Hedrick, J. L.; Dubois, P. *Prog. Polym. Sci.* **2006**, *31*, 723−747. (b) Ikada, Y.; Tsuji, H. *Macromol. Rapid Commun.* **2000**, *21*, 117−132. (c) Uhrich, K. E.; Cannizzaro, S. M.; Langer, R. S.; Shakesheff, K. M. *Chem. Rev.* **1999**, *99*, 3181−3198.

(2) Recent reviews: (a) Wu, J. C.; Yu, T. L.; Chen, C. T.; Lin, C. C. *Coord. Chem. Rev.* **2006**, *250*, 602−626. (b) Dechy-Cabaret, O.; Martin-Vaca, B.; Bourissou, D. *Chem. Rev.* **2004**, *104*, 6147−6176. (c) Lindblad, M. S.; Liu, Y.; Albertsson, A.-C.; Ranucci, E.; Karlsson, S. *Adv. Polym. Sci.* **2002**, *157*, 139−161. (d) O'Keefe, B. J.; Hillmyer, M. A.; Tolman, W. B. *J. Chem. Soc., Dalton Trans.* **2001**, 2215−2224.

(3) (a) Williams, C. K.; Breyfogle, L. E.; Choi, S. K.; Nam, W.; Young, V. G., Jr.; Hillmyer, M. A.; Tolman, W. B. *J. Am. Chem. Soc.* **2003**, *125*, 11350−11359. (b) O'Keefe, B. J.; Breyfogle, L. E.; Hillmyer, M. A.; Tolman, W. B. *J. Am. Chem. Soc.* **2002**, *124*, 4384−4393. (c) Chamberlain, B. M.; Cheng, M.; Moore, D. R.; Ovitt, T. M.; Lobkovsky, E. B.; Coates, G. W. *J. Am. Chem. Soc.* **2001**, *123*, 3229−3238. (d) Stevels, W. M.; Ankone, M. J. K.; Dijkstra, P. J.; Feijen, J. *Macromolecules* **1996**, *29*, 8296−8303. (e) Du, H.; Pang, X.; Yu, H.; Zhuang, X.; Chen, X.; Cui, D.; Wang, X.; Jing, X. *Macromolecules* **2007**, *40*, 1904−1913.

(4) (a) Breyfogle, L. E.; Williams, C. K.; Young, V. G., Jr.; Hillmyer, M. A.; Tolman, W. B. *Dalton Trans.* **2006**, 928−936. (b) Hormnirun, P.; Marshall, E. L.; Gibson, V. C.; Pugh, R. I.; White, A. J. P. *Proc. Natl. Acad. Sci. U.S.A.* **2006**, *103*, 15343−15348. (c) Gregson, C. K. A.; Blackmore, I. J.; Gibson, V. C.; Long, N. J.; Marshall, E. L.; White, A. J. P. *Dalton Trans.* **2006**, 3134−3140. (d) Alcazar-Roman, L. M.; O'Keefe, B. J.; Hillmyer, M. A.; Tolman, W. B. *Dalton Trans.* **2003**, 3082−3087. (e) Chamberlain, B. M.; Cheng, M.; Moore, D. R.; Ovitt, T. M.; Lobkovsky, E. B.; Coates, G. W. *J. Am. Chem. Soc.* **2001**, *123*, 3229−3238.

10.1021/ic700581s CCC: $37.00
Published on Web 07/13/2007

Scheme 1. Pathways for the ROP of Cyclic Esters

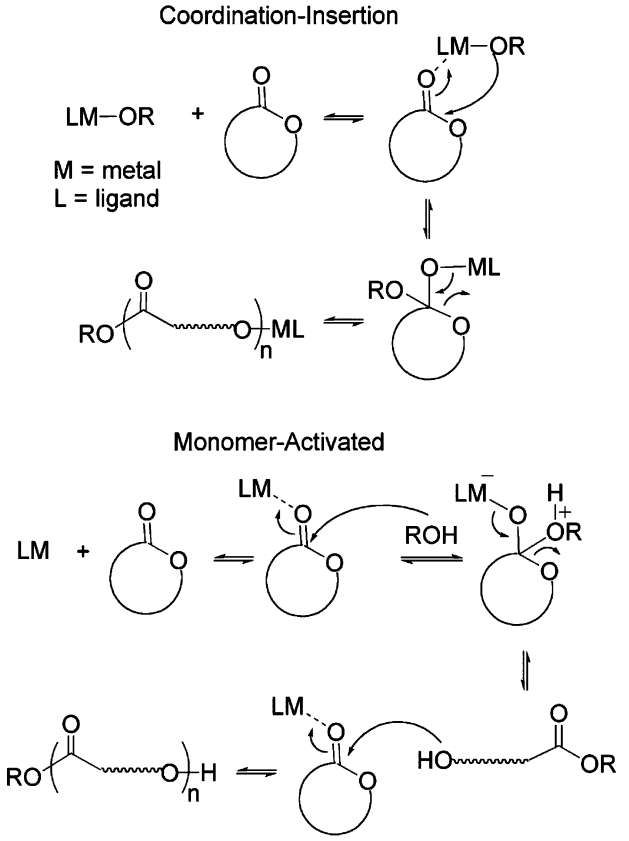

reaction conditions.[6] Advancements pertaining to the monomer-activated pathway have also been achieved through the use of $Sc(OTf)_3$ with protic initiators.[7] In one report,[7a] the ROP of lactide and ϵ-caprolactone (CL) proceeded under mild reaction conditions with low catalyst loadings to yield polyesters of predictable molecular weights. The observed catalytic activity of $Sc(OTf)_3$ was not suppressed in the presence of benzyl alcohol (BnOH), and the resulting polymer molecular weights decreased with increased mole percent of BnOH. Further experiments demonstrated that replacing BnOH with H_2O yielded poly-ϵ-caprolactone (PCL) of analogous molecular weight and provided a one step route for the preparation of telechelic, α-carboxy-ω-hydroxy functionalized PCL.

Given that the future commercial use of polyesters derived from biorenewable resources relies heavily on thorough understanding of synthetic pathways, we sought to identify new, well-defined catalysts that could potentially be used to obtain mechanistic insights and give high polymerization activities. In particular, we focused on developing new variants that would follow the monomer-activated pathway, because it offers several advantages, such as the ability to cap polyester microstructures with biologically relevant end groups (e.g., vitamins, steroidal alcohols, and sugars)[8] without catalyst modification and the potential to exhibit stereochemical control by chain-end or site control mechanisms. Our primary goal is to study potential catalyst/ROH combinations in a comprehensive investigation aimed at identifying the active catalyst and evaluating polymerization activity and mechanism through kinetic studies. An ultimate, albeit daunting, aim is to differentiate coordination-insertion and monomer-activated pathways in a metal/alcohol system. With these objectives in mind, we targeted the synthesis of Zn(II) complexes supported by sterically encumbered bis(phenolato)amine ligands, a choice influenced by previous reports indicating that rapid, controlled, and, in some cases, stereoselective monomer conversion could be achieved with Zn(II) catalysts in the presence of bulky, achiral, ancillary ligands.[3a,c,9] Specific advantages of the selected bis(phenolato)amine ligand frameworks include their availability via reliable, straightforward synthetic preparations offering routine electronic and steric tunability. In addition, the dianionic, tridentate nature of these ligands disfavors ligand dissociation in the presence of added alcohol initiator and concomitant formation of metal−alkoxide units that are active in the coordination-insertion path (instead of a monomer-activated route). The use of related ligands to construct aluminum,[4d,10a,b] calcium,[10c] titanium,[10c] and lanthanide[11] complexes that are active ROP catalysts has recently been reported.

In this contribution, we report the syntheses, characterization, and CL polymerization activity and kinetics of two new Zn(II) complexes of hindered bis(phenolato)amines. Detailed structural studies in the solid state (X-ray crystallography) and in solution (^{1}H NOESY and pulsed gradiant spin-echo NMR experiments) provided insight into the nature of the complexes in resting and catalytically active states. Polymerization experiments, including kinetic studies, were per-

(5) (a) Bourissou, D.; Martin-Vaca, B.; Dumitrescu, A.; Graullier, M.; Lacombe, F. *Macromolecules* **2005**, *38*, 9993−9998. (b) Sanda, F.; Sanada, H.; Shibasaki, Y.; Endo, T. *Macromolecules* **2002**, *35*, 680−683. (c) Shibasaki, Y.; Sanada, H.; Yokoi, M.; Sanda, F.; Endo, T. *Macromolecules* **2000**, *33*, 4316−4320.

(6) (a) Dove, A. P.; Pratt, R. C.; Lohmeijer, B. G. G.; Culkin, D. A.; Hagberg, E. C.; Nyce, G. W.; Waymouth, R. M.; Hedrick, J. L. *Polymer* **2006**, *47*, 4018−4025. (b) Coulembier, O.; Lohmeijer, B. G. G.; Dove, A. P.; Pratt, R. C.; Mespouille, L.; Culkin, D. A.; Benight, S. J.; Dubois, P.; Waymouth, R. M.; Hedrick, J. L. *Macromolecules* **2006**, *39*, 5617−5628. (c) Pratt, R. C.; Lohmeijer, B. G. G.; Long, D. A.; Waymouth, R. M.; Hedrick, J. L. *J. Am. Chem. Soc.* **2006**, *128*, 4556−4557. (d) Lohmeijer, B. G. G.; Pratt, R. C.; Leibfarth, F.; Logan, J. W.; Long, D. A.; Dove, A. P.; Nederberg, F.; Choi, J.; Wade, C.; Waymouth, R. M.; Hedrick, J. L. *Macromolecules* **2006**, *39*, 8574−8583.

(7) (a) Nomura, N.; Taira, A.; Tomioka, T.; Okada, M. *Macromolecules* **2000**, *33*, 1497−1499. (b) Möller, M.; Kange, R.; Hedrick, J. L. *J. Polym. Sci., Part A: Polym. Chem.* **2000**, *38*, 2067−2074.

(8) For relevant examples see: (a) Kricheldorf, H. R.; Damrau, D.-O. *Macromol. Chem. Phys.* **1997**, *198*, 1753−1766. (b) Aigami, K.; Inamoto, Y.; Takaishi, N.; Hattori, K.; Takatsuki, A.; Tamura, G. *J. Med. Chem.* **1975**, *18*, 713−721.

(9) (a) Chisholm, M. H.; Gallucci, J. C.; Phomphrai, K. *Inorg. Chem.* **2005**, *44*, 8004−8010. (b) Chisholm, M. H.; Gallucci, J.; Phomphrai, K. *Inorg. Chem.* **2002**, *41*, 2785−2794. (c) Chisholm, M. H.; Gallucci, J. C.; Zhen, H.; Huffman, J. C. *Inorg. Chem.* **2001**, *40*, 5051−5054. (d) Cheng, M.; Attygalle, A. B.; Lobkovsky, E. B.; Coates, G. W. *J. Am. Chem. Soc.* **1999**, *121*, 11583−11584. (e) Huang, B.-H.; Lin, C.-N.; Hsueh, M.-L.; Athar, T.; Lin, C.-C. *Polymer* **2006**, *47*, 6622−6629.

(10) (a) Chen, C.-T.; Huang, C.-A.; Huang, B.-H. *Dalton Trans.* **2003**, 3799−3803. (b) Tang, Z.; Gibson, V. C. *Eur. Polym. J.* **2007**, *43*, 150−155. (c) Sarazin, Y.; Howard, R. H.; Hughes, D. L.; Humphrey, S. M.; Bochman, M. *Dalton Trans.* **2006**, 340−350.

(11) (a) Delbridge, E. E.; Dugah, D. T.; Nelson, C. R.; Skelton, B. W.; White, A. H. *Dalton Trans.* **2007**, 143−153. (b) Amgoune, A.; Thomas, C. M.; Ilinca, S.; Roisnel, T.; Carpentier, J.-F. *Angew. Chem., Int. Ed.* **2006**, *45*, 2782−2784. (c) Cai, C.-X.; Amgoune, A.; Lehmann, C. W.; Carpentier, J.-F. *Chem. Commun.* **2004**, 330−331.

formed in order to elucidate the influence of catalyst structure, coordinating and noncoordinating solvents, and the concentrations of the catalyst, CL, and BnOH, on the rate and level of control in the ROP of CL. The combined data are consistent with equilibria involving mononuclear and dinuclear forms of the catalyst and a monomer-activated polymerization mechanism.

Experimental Section

All manipulations were performed under an inert atmosphere of N_2 using standard Schlenk line techniques or in a MBraun glovebox. 4-Di-*tert*-butylphenol, methylamine (40% w/w in H_2O), paraformaldehyde (95%), and zinc bis[bis(trimethylsilyl)amide] (97%) were purchased from Aldrich and used as received. Deuterated solvents, dichloromethane (CH_2Cl_2), ϵ-Caprolactone (Aldrich), and BnOH (Acros) were dried over CaH_2, vacuum transferred, and stored in the glovebox. Toluene and tetrahydrofuran were dried over sodium, vacuum transferred, and stored in the glovebox, and all other solvents were purchased commercially and used without further purification. 2-Adamantyl-4-*tert*-butylphenol was synthesized by a previously published procedure.[12] ^{1}H and ^{13}C NMR spectra were recorded on either a Varian VI-300 or Varian VXR-500 spectrometer. The ^{1}H pulsed gradient spin-echo (PGSE) NMR experiments were performed on a Varian INOVA 600 MHz spectrometer equipped with a triple axis gradient unit and a Bioselect triple axis HCN probe with actively shielded gradients. Supression of convection artifacts was achieved using a previously published pulse sequence.[13] Elemental analyses were performed by Robertson Microlit Laboratories, Inc (Madison, NJ). The cosolvent (d_8-THF/CD_2Cl_2) viscosity was determined at 25 °C from the average of three measurements using a Schott Geräte capillary viscometer. Polymer molecular weights (M_n and M_w) and polydispersities were determined by size exclusion chromatography (SEC) with respect to polystyrene standards. All polymer samples were eluted at 40 °C with THF using a flow rate of 1.0 mL/min.

Methylamino-*N*,*N*-bis(2-methylene-4,6-di-*tert*-butylphenol) (H_2L^1) (1). This compound was prepared using a previously published procedure for *N*,*N*-bis(hydroxybenzyl)amines.[14] Methylamine (40% w/w solution in H_2O, 15.0 mL, 0.172 mol) was added dropwise at 0 °C to a stirring solution of paraformaldehyde (10.3 g, 0.334 mol) and potassium hydroxide (86.0 mg, 1.53 mmol) in 52 mL of methanol. After the contents were warmed to ambient temperature, 2,4-di-*tert*-butylphenol (71.0 g, 0.344 mol) in 52 mL of methanol was added in one portion and the reaction was heated at reflux for 24 h. After the reaction mixture was allowed to cool, the volatiles were removed in vacuo (25 °C, 0.15 Torr) and the crude product recrystallized from toluene (4 °C) to afford a white powder (42%, 33.8 g). ^{1}H NMR (δ, CD_2Cl_2): 7.24 (d, $J = 2.3$ Hz, 2H, PhH), 6.95 (d, $J = 2.2$ Hz, 2H, PhH), 3.63 (s, 4H, CH_2), 2.30 (s, 3H, CH_3), 1.40 (s, 18H, ^{t}Bu), 1.28 (s, 18H, ^{t}Bu). ^{13}C NMR (δ, CD_2Cl_2): 153.0, 142.2, 136.5, 125.6, 124.1, 122.4, 60.4, 42.3, 35.3, 34.6, 31.9, 30.0. Anal. Calcd for $C_{31}H_{49}NO_2$: C, 79.59; H, 10.58; N, 2.99. Found: C, 79.59; H, 10.77; N, 2.89.

Methylamino-*N*,*N*-bis(2-methylene-4-adamantyl-6-*tert*-butylphenol), (H_2L^2) (2). Methylamine (40% w/w solution in H_2O, 2.30 mL, 0.0262 mol) was added dropwise at 0 °C to a stirring solution of paraformaldehyde (1.57 g, 0.0524 mol) and potassium hydroxide (13.1 mg, 0.233 mmol) in 10 mL of methanol. After the contents were allowed to warm to ambient temperature, 2-adamantyl-4-*tert*-butylphenol (14.9 g, 0.0524 mol) in 20 mL of methanol was added in one portion and the reaction was heated at reflux for 24 h. The resulting white precipitate was collected by filtration, dried in vacuo (25 °C, 0.20 Torr), and recrystallized from hexane at 4 °C (39%, 6.38 g). ^{1}H NMR (δ, CD_2Cl_2): 7.19 (d, $J = 2.3$ Hz, 2H, PhH), 6.95 (d, $J = 2.2$ Hz, 2H, PhH), 3.62 (s, 4H, CH_2), 2.33 (s, 3H, CH_3), 2.14 (s, 12H, CH_2-adamantyl), 2.05 (bs, 6H, CH-adamantyl), 1.77 (s, 12H, CH_2-adamantyl), 1.28 (s, 18H, ^{t}Bu). ^{13}C NMR (δ, CD_2Cl_2): 153.2, 142.4, 137.0, 125.5, 124.0, 122.7, 60.0, 42.4, 41.1, 37.7, 34.7, 31.9, 30.0. Anal. Calcd for $C_{43}H_{61}NO_2$: C, 82.75; H, 9.87; N, 2.25. Found: C, 82.98; H, 10.05; N, 1.94.

$Zn_2(L^1)_2$ (3). H_2L^1 (2.81 g, 6.18 mmol) in toluene (14 mL) was added to a stirring solution of $Zn[N(TMS)_2]_2$ (2.39 g, 6.18 mmol) in toluene (7 mL). The resulting yellow mixture was stirred at room temperature for 14 h and subsequently dried under vacuum (25 °C, 0.20 Torr). The resulting yellow solid was washed with 3 × 15 mL of hexanes yielding a white powder (75%, 2.46 g). X-ray quality crystals were obtained from a saturated CH_2Cl_2 solution at −38 °C. ^{1}H NMR (δ, CD_2Cl_2): 7.30 (s, 2H, PhH), 7.09 (s, 2H, PhH), 7.02 (s, 2H, PhH), 6.70 (s, 2H, PhH), 4.98 (d, $J = 13$ Hz, 2H, CH_2), 3.90 (d, $J = 13$ Hz, 2H, CH_2), 3.40 (d, $J = 13$ Hz, 2H, CH_2), 2.59 (s, 6H, NCH_3), 2.57 (d, $J = 13$ Hz, 2H, CH_2), 1.39 (s, 18H, ^{t}Bu), 1.29 (s, 18H, ^{t}Bu), 1.20 (s, 18H, ^{t}Bu), 1.18 (s, 18H, ^{t}Bu). ^{13}C NMR (δ, CD_2Cl_2): 162.4, 157.5, 142.6, 138.9, 138.3, 136.7, 127.6, 126.5, 125.6, 124.7, 124.4, 120.7, 65.3, 61.1, 47.1, 35.7, 35.5, 34.6, 34.3, 32.1, 31.8, 31.4, 29.7. Anal. Calcd for $C_{62}H_{94}N_2O_4Zn_2$: C, 70.09; H, 8.94; N, 2.64. Found: C, 70.31; H, 8.88; N, 2.54.

$Zn_2(L^2)_2$ (4). H_2L^2 (2.00 g, 3.20 mmol) in toluene (14 mL) was added to a stirring solution of $Zn[N(TMS)_2]_2$ (1.24 g, 3.20 mmol) in toluene (7 mL). The yellow mixture was stirred at room temperature for 24 h and subsequently dried under vacuum (25 °C, 0.20 Torr). The sticky, yellow crude product was suspended in 10 mL of hexanes and cooled to −40 °C for 3 h. The resulting precipitate was collected via filtration yielding **4** as white powder (78%, 1.72 g). X-ray quality crystals were obtained from a saturated toluene solution at −38 °C. ^{1}H NMR (δ, CD_2Cl_2): 7.31 (s, 2H, PhH), 7.05 (s, 2H, PhH), 6.96 (s, 2H, PhH), 6.68 (s, 2H, PhH), 5.22 (d, $J = 13$ Hz, 2H, CH_2), 3.97 (d, $J = 13$ Hz, 2H, CH_2), 3.42 (d, $J = 13$ Hz, 2H, CH_2), 2.60 (d, $J = 13$ Hz, 2H, CH_2), 2.58 (s, 6H, NCH_3), 2.11 (m, 24H, CH_2-adamantyl), 1.93 (s, 6H, CH-adamantyl), 1.82 (s, 6H, CH-adamantyl), 1.68 (m, 24H, CH_2-adamantyl), 1.28 (s, 18H, ^{t}Bu), 1.21 (s, 18H, ^{t}Bu). ^{13}C NMR (δ, CD_2Cl_2): 163.1, 158.3, 142.2, 139.1, 138.5, 137.1, 127.5, 126.6, 126.5, 124.6, 124.5, 120.7, 65.6, 60.9, 45.4, 42.7, 41.0, 39.3, 38.0, 37.9, 37.3, 34.5, 34.3, 32.2, 32.1, 31.8, 30.0, 29.5, 23.2, 14.4. Anal. Calcd for $C_{86}H_{118}N_2O_4Zn_2$: C, 75.13; H, 8.67; N, 2.04. Found: C, 75.42; H, 8.82; N, 1.75.

X-ray Crystallography. Single crystals of **3** and **4** suitable for X-ray diffraction were coated with Paratone N, attached to a glass fiber, and mounted on a Bruker SMART platform CCD diffractometer for collection at 173(2) K. A preliminary set of unit cell constants were collected from three sets of 20 frames. The initial sets of frames were orientated such that orthogonal wedges of reciprocal space were surveyed, resulting in initial orientation matrices determined from 164 (**3**) or 93 (**4**) reflections. Data collection was performed using Mo Kα radiation with a frame time of 15 and 45 s for **3** and **4**, respectively, and a detector distance of 4.987 cm. A randomly orientated region of reciprocal space was analyzed to the extent of one sphere and to a resolution of 0.77 Å

(12) Aigami, K.; Inamoto, Y.; Takaishi, N.; Hattori, K. *J. Med. Chem.* **1975**, *18*, 713−721.
(13) Jerschow, A.; Müller, N. *J. Magn. Reson.* **1997**, *125*, 372−375.
(14) Burke, W. J.; Smith, R. P.; Weatherbee, C. *J. Am. Chem. Soc.* **1952**, *74*, 602−605.

(**3**) or 0.84 Å (**4**). Four major sections of frames were collected with 0.30° steps in ω at four different ϕ settings and a detector position of −28° in 2θ. The intensity data were corrected for absorption and decay.[15] Final cell constants were calculated from the *xyz* centroids of 3347 (**3**) or 3410 (**4**) strong reflections from the data collection following integration (SAINT).[16] The structures of **3** and **4** were solved using SHELXS-97 and refined using SHELXL-97.[17] The space groups $P2(1)/n$ (**3**) and $P\bar{1}$ (**4**) were determined based on systematic absences and intensity statistics. A direct methods solution was determined for **3** and **4**[18] which successfully located most of the non-hydrogen atoms from the E-map. Full-matrix least-squares/difference Fourier cycles were performed to locate the remaining non-hydrogen atoms using SHELXTL-97. All non-hydrogen atoms were refined with anisotropic displacement parameters, while all hydrogen atoms were placed in ideal positions and refined as riding atoms with relative isotropic displacement parameters. Compound **4** contained two lattice toluene solvent molecules, one of which could not be sufficiently modeled in the refinement cycles and was removed using the function SQUEEZE from the program PLATON.[19]

Typical Procedure for K_{eq} Determinations. In the glovebox, **3** (99.0 mg, 0.0932 mmol), substrate (CL, THF, or BnOH), and trimethoxybenzene (TMB, internal standard) were sequentially added to a 1 mL volumetric flask. The contents of the volumetric flask were dissolved in CD_2Cl_2 and diluted to a final volume of 1 mL with CD_2Cl_2. The solution was transferred to a J-Young NMR tube, capped, and removed from the glovebox. A ^{1}H NMR spectrum was collected on a 500 MHz NMR spectrometer at 25 °C using a delay time of 20 s. The concentrations used to determine each K_{eq} value were calculated from the peak areas corresponding to monomer (LZnS) (6.87 ppm), dimer (L_2Zn_2) (6.73 ppm), and substrate (S) (CL = 4.20 ppm; THF = 1.85 ppm; BnOH = 4.63 ppm) relative to TMB (6.10 ppm). The K_{eq} value obtained for each substrate was calculated from the average of three independent measurements at a fixed substrate concentration. Accurate calculation of K_{eq} when BnOH was employed as the substrate was complicated by substantial peak overlap in the ^{1}H NMR spectrum. Therefore, the equilibrium constant determined from three independent measurements with constant $[BnOH]_0$ (K_{eq} = 72 M^{-1}) is an estimation of the actual experimental value. An additional set of experiments was performed to verify the reproducibility of K_{eq} for BnOH. A K_{eq} value of 77 M^{-1} was calculated from the average of three independent measurements at variable $[BnOH]_0$ ($[BnOH]_0$ = 0.04, 0.08, 0.13 M; $[Zn]_0$ = 0.186 M). The final equilibrium constant (K_{eq}) for BnOH (see text) is the average value calculated from all six measurements. The numbers in parentheses (see text) represent the estimated standard deviation for the experimentally determined K_{eq} values.

General Procedure for ϵ-Caprolactone Polymerization. In the glovebox, a vial containing a magnetic stir bar was charged with ϵ-caprolactone (1.22 g, 10.7 mmol). While the contents were being stirred at 25 °C, the initiator and catalyst solution in THF were added successively, and the vial was tightly capped. At certain intervals of time during the reaction, two drops of the reaction mixture were removed and dissolved in $CDCl_3$ and monitored via ^{1}H NMR spectroscopy. After acheiving >85% conversion as determined by ^{1}H NMR spectroscopy, the polymerizations were quenched with 2 drops of H_2O and the polymers precipitated in *n*-hexane. The *n*-hexane/H_2O was decanted, and the polymer was dried in vacuo overnight. The dry polymer was then dissolved in CH_2Cl_2, reprecipitated with *n*-hexane, and dried to a constant weight prior to analyses by SEC.

Representative Procedure for Initial Rate Determinations. In the glovebox, **3** (99.0 mg, 0.0932 mmol), CL (171 mg, 166 μL, 1.50 mmol), and benzyl alcohol (14.1 mg, 13.5 μL, 0.130 mmol) were successively added to a 1 mL volumetric flask. The contents of the volumetric flask were dissolved in CD_2Cl_2 and diluted to a final volume of 1 mL with CD_2Cl_2. The solution was transferred to a J-Young NMR tube, capped, and removed from the glovebox. ^{1}H NMR spectra were collected on a 500 MHz NMR spectrometer at 25 °C every 30 s over a period of 210 s resulting in eight data points. The remaining concentration of CL at each 30 s time interval ($[CL]_t$) was determined from peaks corresponding to PCL growth (3.93 ppm) and CL decay (4.20 ppm); the percentage of remaining CL after 210 s was 99.5% at $[CL]_0$ = 0.400 M and 97.0% at $[CL]_0$ = 5.00 M. The eight data points were plotted ($[CL]_t$ vs time (s)), and the initial rate of polymerization (R_p) was determined from the slope of a linear fit to the data. Initial rate experiments were performed over a range of $[CL]_0$ (0.400−5.00 M) with $[Zn]_0$ and $[BnOH]_0$ fixed at 0.186 and 0.130 M, respectively, and replicate runs were performed for each $[CL]_0$ to confirm reproducibility. The initial rates of polymerization were subsequently plotted versus $[CL]_0$ as shown in Figure 6a. The reaction conditions used for all initial rate experiments are detailed in the caption of Figure 6. All kinetics plots and linear curve fits were generated using KaleidaGraph version 3.6 or 4.0.

Results and Discussion

(a) Synthesis and Characterization of Complexes. The proligands methylamino-*N*,*N*-bis(2-methylene-4,6-di-*tert*-butylphenol) (**1**, R′ = ^{t}Bu) and methylamino-*N*,*N*-bis(2-methylene-4-adamantyl-6-*tert*-butylphenol) (**2**, R′ = adamantyl) were prepared by Mannich condensation of methylamine, paraformaldehyde, and the respective substituted phenol in refluxing methanol.

Stoichiometric reaction of $Zn[N(TMS)_2]_2$ with **1** and **2** in toluene at ambient temperature afforded **3** and **4**, respectively (Scheme 2). Compounds **3** and **4** were characterized by ^{1}H and ^{13}C NMR spectroscopy, elemental analysis, and X-ray crystallography. The solid-state structures of compounds **3** and **4**, including relevant bond lengths and angles, are depicted in Figures 1 and S1 (Supporting Information), respectively. Both **3** and **4** adopt dinuclear structures, with each Zn(II) ion coordinated to one bis(phenolato)amine ligand that uses one oxygen and one nitrogen atom to bind in a terminal fashion and the other phenolate to bridge between the metal ions. The bridging phenolate binds asymmetrically, with Zn1−O(2) and Zn1−O(2A) bond distances of 2.022(1) and 1.953(1) Å for **3** and 2.022(1) and 1.954(1) Å for **4**. The coordination geometries in **3** and **4** are best described as distorted tetrahedral, as illustrated by O1−Zn1−O2A and O2−Zn−O2A bond angles of 124.16(6)° and 84.54(5)° for **3** and 122.33(9)° and 85.68(9)°

(15) Blessing, R. H. *Acta Crystallogr.* **1995**, *A51*, 33−38.
(16) *SAINT+ V6.45*; Bruker Analytical X-ray Systems: Madison, WI 2003.
(17) *SHELXTL V6.14*; Bruker Analytical X-ray Systems: Madison, WI 2000.
(18) Altomare, A.; Burla, M. C.; Camalli, M.; Cascarano, G.; Giacovazzo, C.; Guargliardi, A.; Moliterni, A. G. G.; Polidori, G.; Spagna, R. *J. Appl. Crystallogr.* **1999**, *32*, 115−119.
(19) (a) Spek, A. L. *Acta Crystallogr.* **1990**, *A46*, C34. (b) Spek, A. L. *PLATON, A Multipurpose Crystallographic Tool*; Utrecht University: Utrecht, The Netherlands 2000.

Scheme 2. Synthesis of Complexes **3** and **4** (S = THF)

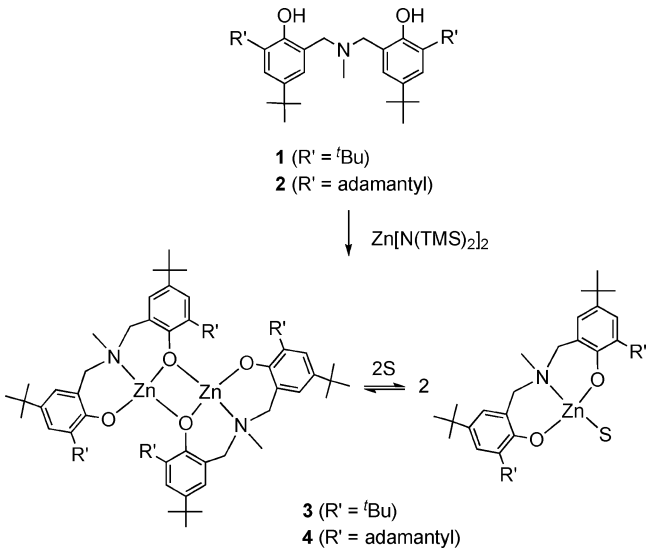

for **4**. The Zn(1)−Zn(1A) separations of 2.9418(4) Å for **3** and 2.9022(7) Å for **4** are in good agreement with previously described dizinc complexes containing μ-O(phenolate) bridges.[9e,20]

^{1}H NMR spectra of compounds **3** and **4** in CD_2Cl_2 at ambient temperature support retention of the dinuclear structures determined by X-ray diffraction. Thus, they exhibit four well-resolved aromatic signals and four signals for the diastereotopic methylene hydrogens, consistent with two symmetry-related bridging and terminally coordinated phenolato groups. Entirely different spectra are observed for **3** and **4** in d_8-THF, wherein a distinct pattern of two aromatic and two diastereotopic methylene signals are observed. This pattern is consistent with a monomeric species "L^{1}Zn" resulting from cleavage of the dinuclear complex by the solvent. When d_8-THF was added in portions (5−40 equiv) to a CD_2Cl_2 solution of **3**, the pattern of signals corresponding to dimeric **3** decreased in intensity, whereas those signals consistent with the putative monomeric complex increased (Figure 2). Upon addition of 40 equiv of d_8-THF, resonances consistent with the monomeric form of **3** were exclusively observed. These data support an equilibrium between monomeric and dimeric forms involving THF (Scheme 2). Working under this assumption, a K_{eq} value of 0.33(2) M^{-1} was determined from integration of NMR spectra (see Experimental Section). Similarly, peaks attributable to dimeric and monomeric species were observed in ^{1}H NMR spectra of **3** in CD_2Cl_2 with added CL or BnOH, and K_{eq} values for these equilibria were determined to be 6(1) × 10^{-3} M^{-1} and 74(8) M^{-1}, respectively.

To verify the postulated monomer−dimer equilibria and assign the ^{1}H NMR resonances, a ^{1}H−^{1}H NOESY spectrum of complex **3** was obtained at room temperature in CD_2Cl_2 (0.169 M) with 10 equiv of added d_8-THF. Only the aromatic region of the spectrum is depicted in Figure 3 for clarity. Peak assignments for dimeric **3** (**A, B**) and its mononuclear form (**C**, **C′**) were determined from cross signals arising from spatial proximity of the aromatic protons ($\mathbf{A_t}$ and $\mathbf{A_b}$ for dimeric **3**, **C** for the mononuclear form of **3**) and the flanking ^{t}Bu groups (data not shown). The intense cross-peaks labeled X arise from chemical exchange between aromatic protons $\mathbf{A_t} \leftrightarrow \mathbf{A_b}$ and $\mathbf{B_t} \leftrightarrow \mathbf{B_b}$, which we attribute to a fluxional process involving switching of the phenolate donors between terminal and bridging positions in the dimer. Most importantly, firm evidence that the two forms of **3** rapidly equilibrate is provided by the presence of additional cross-peaks labeled Y, which correspond to exchange between protons $\mathbf{A_t}/\mathbf{A_b} \leftrightarrow \mathbf{C}$ and $\mathbf{B_t}/\mathbf{B_b} \leftrightarrow \mathbf{C'}$.

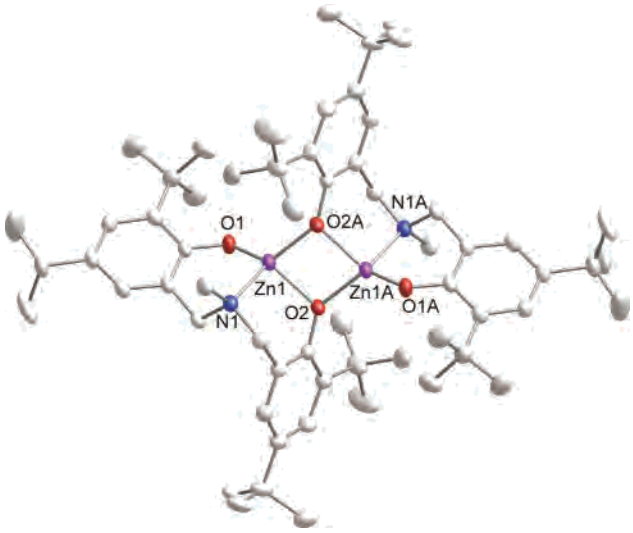

Figure 1. X-ray structure of **3** as 50% thermal ellipsoids with hydrogen atoms omitted for clarity. Selected bond distances (Å) and angles (deg) for **3**: Zn1−O1, 1.865(1); Zn1−O2, 2.022(1); Zn1−O2A, 1.953(1); Zn1−N1, 2.063(2); Zn1−Zn1A, 2.9418(4); O1−Zn1−O2, 123.38(6); O1−Zn1−O2A, 124.16(6); O2−Zn1−O2A, 84.54(5); O1−Zn1−N1, 102.77(6); O2−Zn1−N1, 95.15(6); O2A−Zn1−N1, 123.52(6). Selected bond distances and angles for **4**: Zn1−O1, 1.856(2); Zn1−O2, 2.022(2); Zn1−O2A, 1.954(2); Zn1−N1, 2.049(2); Zn1−Zn1A, 2.9159(7); O1−Zn1-O2, 120.91(10); O1−Zn1−O2A, 122.33(9); O2−Zn1−O2A, 85.68(9); O1−Zn−N1, 101.05(10), O2−Zn1−N1, 93.18(9); O2A−Zn1−N1, 129.77(10).

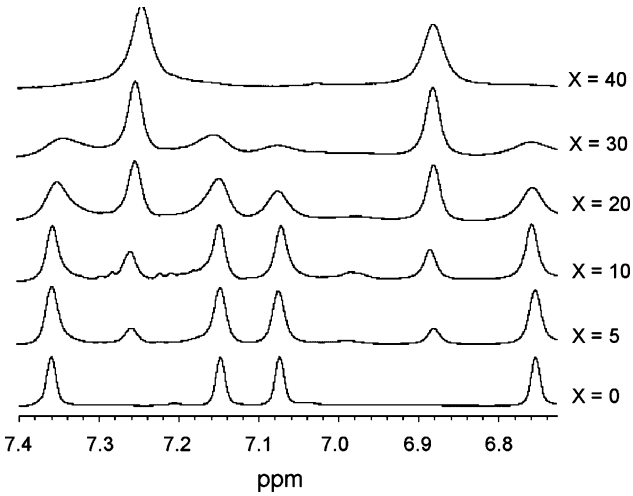

Figure 2. ^{1}H NMR spectrum of the aromatic region of **3** in CD_2Cl_2 (0.169 M) with the indicated number of equivalents (X relative to dimeric **3**) of added d_8-THF.

(20) (a) Darensbourg, D. J.; Rainey, P.; Yarbrough, J. *Inorg. Chem.* **2001**, *40*, 986−993. (b) Kunert, M.; Bräuer, M.; Klobes, O.; Görls, H.; Dinjus, E.; Anders, E. *Eur. J. Inorg. Chem.* **2000**, 1803−1809. (c) Hlavinka, M. L.; McNevin, M. J.; Shoemaker, R.; Hagadorn, J. R. *Inorg. Chem.* **2006**, *45*, 1815−1822.

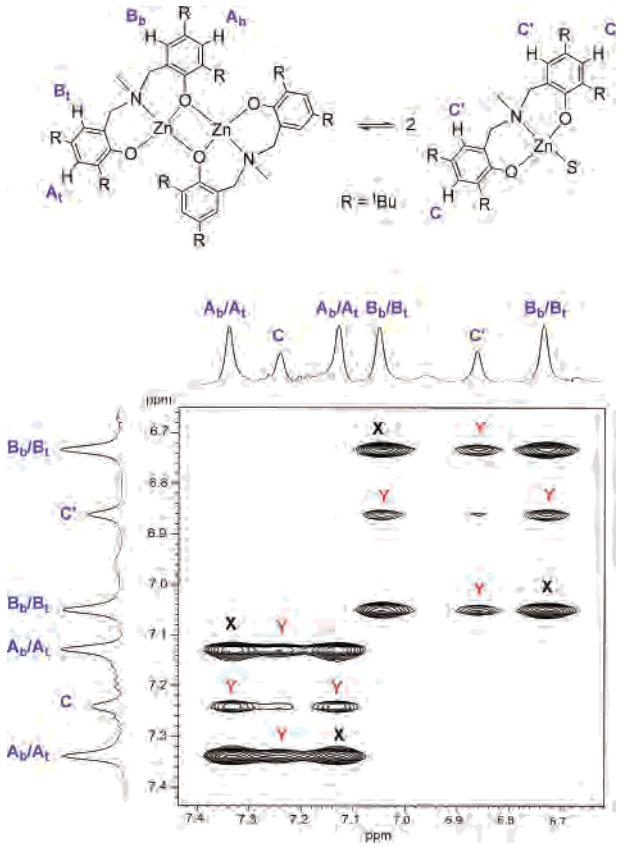

Figure 3. ^{1}H−^{1}H NOESY spectrum and assignments for **3** in CD_2Cl_2 with added d_8-THF in the aromatic region. Conditions: 25 °C, [**3**] = 0.169 M, with 10 equiv of d_8-THF added. The peaks marked by a black "X" are attributed to chemical exchange due to a fluxional process that interconverts the bridging and terminal phenolate arms of the ligand in dimeric **3**, while those marked by a red "Y" are attributed to chemical exchange due to the indicated monomer−dimer equilibrium.

The nuclearity of the species observed upon addition of d_8-THF to a CD_2Cl_2 solution of **3** was confirmed through a pulsed gradient spin-echo (PGSE) NMR experiment, an established technique that has been used to estimate the diffusion coefficient (i.e., size) of a wide variety of molecules in solution.[21] This experiment was performed on **3** in CD_2Cl_2 (1.69 M) at 25 °C with 10 equiv of added d_8-THF. The diffusion coefficients of **3** in CD_2Cl_2 and monomer in d_8-THF could theoretically be measured in separate experiments taking solvent viscosity into account based on the Stokes−Einstein equation (eq 1, where D = diffusion coefficient, η = viscosity, and r = effective hydrodynamic radius). However, we chose the aforementioned CD_2Cl_2/d_8-THF solvent mixture because aromatic signals consistent with **3** and the monomer are both present and well-resolved. Thus, the diffusion coefficients of both species could be determined in a single experiment with identical solvent viscosity and at the same temperature. The plot of $\ln(I/I_o)$ (I = observed spin-echo intensity; I_o = intensity in the absence of gradients) versus the square of the gradient amplitude is shown in Figure 4. Each data point corresponds to the average intensities obtained from the ^{1}H NMR spectrum over a range

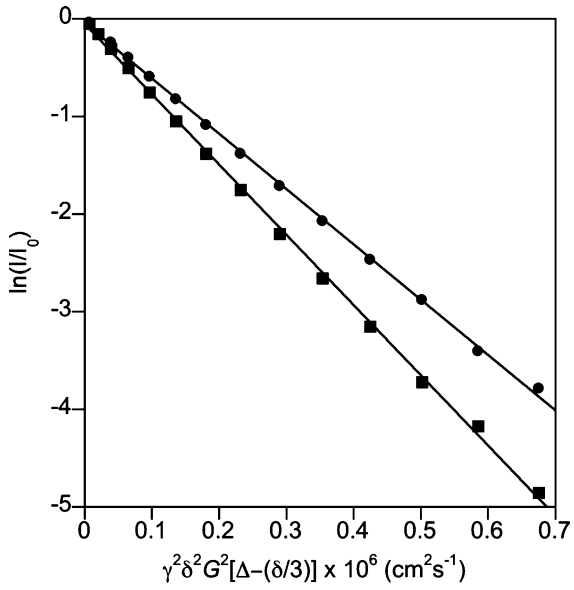

Figure 4. Plot of pulsed gradient spin-echo (PGSE) NMR data for **3** (dimer, circles; monomer, squares). The lines are fits to eq 2, and the slope is proportional to the diffusion coefficient, D.

of gradient strengths. The slope of each best-fit line to eq 2 is proportional to the diffusion coefficient, D, where G = gradient strength, Δ = delay between midpoints of the gradients, δ = length of gradient pulse, and γ = gyromagnetic ratio. From the experimental PGSE data, diffusion coefficients of 5.7×10^{-6} cm^2 s^{-1} (**3**, dimer) and 7.2×10^{-6} cm^2 s^{-1} (monomer) were determined in the CD_2Cl_2/d_8-THF cosolvent mixture. The ∼20% increase in diffusion coefficient for the monomer supports its assigned nuclearity.[22]

$$D = \frac{kT}{6\pi\eta r} \tag{1}$$

$$\ln(I/I_0) = -\gamma^2\delta^2G^2[\Delta - (\delta/3)]D \tag{2}$$

Further support for this conclusion was obtained by calculating the hydrodynamic radius of dimeric **3** (r'_{dimer}) from the X-ray structure and estimating the hydrodynamic radius for a mononuclear species ($r'_{monomer}$) based on one-half of **3** with a THF molecule coordinated to the Zn(II) center.[23] Since dimeric **3** and a mononuclear-THF adduct (L^1Zn(THF)) of **3** both approximate the shape of prolate ellipsoids, eq 3[24] was used to determine the corresponding radii, with a and b representing the major and minor axes of the molecular structures, respectively. The calculated hydrodynamic radii values obtained from the X-ray structure of **3** and a hypothetical monomer-THF adduct (L^1Zn(THF)) were 8.8 and 5.0 Å, respectively. For comparison, the hydrodynamic radii were then determined (eq 1) from the

(21) Pregosin, P. S. *Prog. Nucl. Magn. Reson. Spectrosc.* **2006**, *49*, 261−288.

(22) (a) Valentini, M.; Rüegger, H.; Pregosin, P. S. *Helv. Chim. Acta* **2001**, *84*, 2833−2853. (b) Jiang, Q.; Rüegger, H.; Venanzi, L. M. *Inorg. Chim. Acta* **1999**, *290*, 64−79.

(23) The hydrodynamic radius calculated for one-half of **3** without coordinated THF molecules was 3.0 Å.

(24) Price, W. S. In *New Advances in Analytical Chemistry*; Rahman, A., Ed.; Hardwood Academic Publishers: Singapore, 2000; pp 31−72.

Table 1. Results for the Polymerization of CL with **3** and **4**[a]

catalyst	$[CL]_0$:$[Zn]_0$:$[BnOH]_0$	time (min)	M_n(calcd)[b] (kg mol^{-1})	M_n(NMR)[c] (kg mol^{-1})	M_n(SEC)[d] (kg mol^{-1})	PDI[d]	conversion (%)
3	50:2:0	360					<5
3	50:2:2	360	2.6	3.5	4.0	1.09	92
3	50:2:2.7	320	1.9	2.7	3.3	1.14	90
3	50:2:3.1	300	1.6	2.2	2.6	1.20	99
3	50:2:4	240	1.3	1.7	1.7	1.24	91
3	50:2:8	90	0.68	0.94	1.1	1.22	96
3	50(50):2:2[e]	490	5.6	7.6	10.8	1.13	98
3	100:2:2	480	5.5	4.6	9.6	1.08	97
3	100:2:4	300	2.7	3.2	5.1	1.09	96
3	100:2:8	170	1.3	1.6	2.1	1.16	94
4	50:2:0	130					<5
4	50:2:2	130	2.6	3.0	4.2	1.11	90
4	50:2:2.7	115	1.9	2.7	3.0	1.18	89
4	50:2:3.1	115	1.6	2.1	2.4	1.15	86
4	50:2:4	105	1.3	1.6	2.5	1.14	90
4	50:2:8	70	0.61	0.85	0.95	1.12	86
4	50(50):2:2[e]	250	5.5	6.3	10.4	1.16	97

[a] Conditions: 25 °C, THF, $[CL]_0 = 4.73$ M, $[Zn]_0 = 0.400$ M. [b] Calculated from the mol wt of CL × $[CL]_0/[BnOH]_0$ × % conversion. [c] Determined from integration of ^{1}H NMR spectra assuming one −OBn group per chain. [d] Determined by SEC vs polystyrene standards. [e] Additional 50 equiv CL added after initial run.

experimental PGSE results. First, the solvent viscosity ($\eta_{cosolvent}$) for the d_8-THF/CD_2Cl_2 solvent mixture was determined to be 0.420 cP from eq 4[25] based on an average of three measurements with a capillary viscometer using water as a standard (ρ = density, Δt = time to deliver a known volume). From the diffusion coefficients obtained experimentally for **3** ($D_{dimer} = 5.7 \times 10^{-6}$ cm^2 s^{-1}) and L^{1}Zn(THF) ($D_{monomer} = 7.2 \times 10^{-6}$ cm^2 s^{-1}) and the calculated cosolvent viscosity (eq 4), the hydrodynamic radii for **3** (r_{dimer}) and a monomeric-THF complex ($r'_{monomer}$) were calculated from eq 1 to be 9.2 and 5.8 Å, respectively. The agreement between these values and those estimated from the X-ray data strongly support the hypothesis that dimer **3** is cleaved by added THF into a monomer, most likely solvated L^{1}Zn(THF). Attempts to obtain X-ray quality crystals of L^{1}Zn(THF) via recrystallization of **3** from THF were unsuccessful.

$$r' = (ab^2)^{1/3} \tag{3}$$

$$\eta_{cosolvent} = \frac{\rho_{cosolvent}}{\rho_{H_2O}} \frac{\Delta t_{cosolvent}}{\Delta t_{H_2O}} \eta_{H_2O} \tag{4}$$

(b) Polymerization of CL. Ring-opening polymerizations of CL initiated with BnOH in the presence of **3** and **4** were performed at 25 °C in THF (Table 1). Although somewhat low $[CL]_0/[Zn]_0$ ratios and high $[CL]_0$ (4.73 M) were necessary to achieve >85% monomer conversion in reasonable reaction times, narrow PDIs (1.08−1.24) and predictable molecular weights were obtained for all polymerizations catalyzed by **3** and **4** over a range of added BnOH (2, 2.7, 3.1, 4, and 8 equiv relative to dimeric **3**). A linear relationship between the PCL number-average molecular weight (M_n) and $([CL]_0 - [CL]_t)/[BnOH]_0$ (Figure 5) is indicative of a controlled polymerization process. This conclusion was further supported by observation of consumption of an additional 50 equiv of CL after the initial conversion of 50 equiv of monomer (Supporting Information, Figure S2). A systematic comparison of **3** and **4** using a $[CL]_0/[Zn]_0$ ratio of 50:2 (Table 1) suggests higher activity using **4** relative to **3** under the identical polymerization conditions (90% monomer conversion with **4** after 130 min, 92% conversion using **3** after 360 min) and indicate that increasing the sterics at the ligand periphery from ^{t}Bu (**3**) to adamantyl (**4**) results in enhanced polymerization rates. Like **3**, we suspect that dimer **4** is also cleaved into two monomeric THF adducts (L^{2}Zn(THF)). However, in the case of **4**, the bulky adamantyl substituents render a more sterically encumbered Zn(II) center having a bound THF molecule that is more readily displaced by CL in the polymerization process. This postulate assumes a monomer-activated pathway and implies that THF inhibits substrate coordination and polymerization.

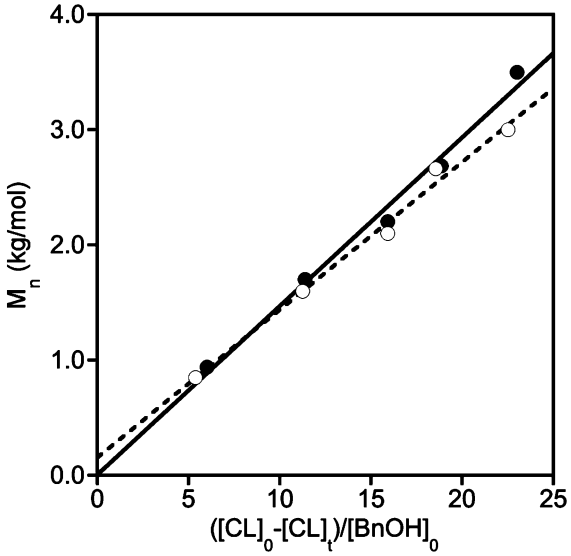

Figure 5. Plots of M_n (NMR) vs $([CL]_0 - [CL]_t)/[BnOH]_0$ using **3** (solid circles) or **4** (empty circles) as catalyst, with linear fits (solid, $R = 0.994$, and dashed, $R = 0.995$, lines, respectively). Conditions: $[CL]_0 = 4.73$ M, $[Zn]_0 = 0.40$ M, THF, 25 °C.

(25) Hiemenz, P. C.; Lodge, T. P. *Polymer Chemistry*, 2nd ed.; Taylor and Francis: Boca Raton, FL, 2007.

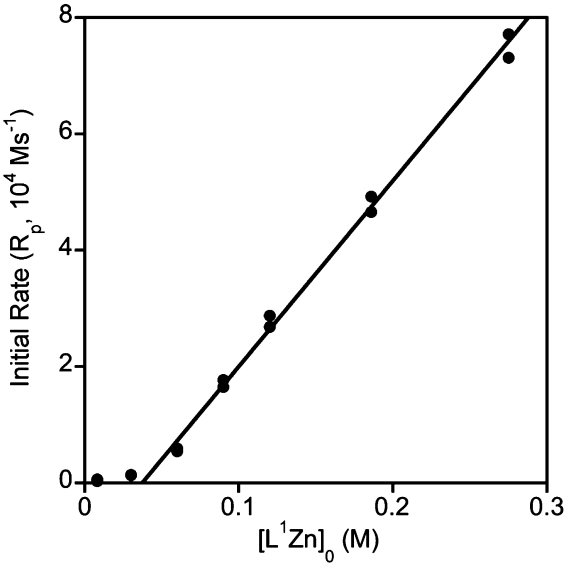

Figure 6. Plot of the initial rate of polymerization of CL vs the initial concentration of L^1Zn (twice the amount of added **3**) in CD_2Cl_2 at 25 °C. Conditions: $[CL]_0 = 1.5$ M, $[BnOH]_0 = 0.13$ M, CD_2Cl_2, 25 °C. The indicated linear fit excludes the data points below $[L^1Zn]_0 = 0.05$ M and is characterized by slope $= 3.19 \times 10^{-3}$ s^{-1}, *x*-intercept = 0.0374 M, and $R = 0.998$.

Kinetic studies were performed with **3** in an attempt to gain insight into the CL polymerization pathway in the presence of added BnOH initiator and to test the hypothesis of THF inhibition. Initial rates of polymerization (R_p) were determined by monitoring CL conversion versus time by ^1H NMR spectroscopy in CD_2Cl_2 with various initial concentrations of CL, BnOH, and catalyst. In one set of experiments, fixed initial concentrations $[CL]_0 = 1.5$ M and $[BnOH]_0 = 0.130$ M were used while $[L^1Zn]_0$ ($2 \times [\mathbf{3}]_0$) was varied (Figure 6). The good linear fit of the data for $[L^1Zn]_0 > 0.05$ M is consistent with a first-order dependence of R_p on $[L^1Zn]$. The nonzero *x*-intercept of 0.0374 M suggests a threshold catalyst concentration below which catalysis is inhibited significantly, a precedented phenomenon[3a] attributable to a low-level deactivating impurity, here corresponding to 2.5% of $[CL]_0$. Further support for such catalyst deactivation was found in experiments performed with fixed concentrations $[L^1Zn]_0 = 0.186$ M and $[BnOH]_0 = 0.130$ M and varying $[CL]_0$ (0.400−5.00 M) (Figure 7).[26] For $[CL]_0 \leq 2.0$ M, a plot of R_p versus [CL] may be fit well ($R = 0.994$) to a straight line with a slope $= 3.22$ s^{-1} and an *x*-intercept of 0.139 M (Figure 7a). This indicates a first-order dependence of R_p on [CL] with a nonzero *x*-intercept suggesting that this small amount of CL (just below $[L^1Zn]_0$ and approximately equal to $[BnOH]_0$) is somehow "unavailable" for polymerization. In other words, the actual amount of CL free for polymerization is $[CL]_0' = [CL]_0 - 0.139$ M (where $[CL]_0$ refers to the amount of CL initially added). Such nonzero *x*-intercepts in plots of R_p versus monomer concentration have been interpreted to represent the equilibrium monomer concentration ($[M]_{eq}$),[27] but $[CL]_{eq}$ is known to be 0.007 M at 25 °C,[28] a value ~20-fold smaller than the *x*-intercept in Figure 7a. Thus, we are currently unable to unambiguously attribute the cause of the nonzero intercept and can only speculate that it represents a relatively small amount of CL that is bound in nonproductive species.[29]

Considering the full range of $[CL]_0$ values (Figure 7b), the rate apparently saturates at $[CL]_0 > 2.0$ M and even appears to slow above $[CL]_0 \sim 4$ M. An obvious explanation of this would be preequilibrium binding of the substrate prior to ring opening, but an attempted fit of the data to the appropriate Michaelis−Menton expression was unsuccessful (Supporting Information, Figure S3). An alternative rationale that is also consistent with that used to explain the nonzero intercept in Figure 6 is catalyst deactivation by an impurity, the amount of which is proportional to $[CL]_0$ (more deactivating impurity at larger $[CL]_0$). According to this hypothesis, the effective concentration of catalyst, $[L^1Zn]_{eff}$, can be expressed by eq 5, where *f* is the fraction of $[CL]_0'$ that is responsible for deactivation of the catalyst. Substitution of this expression into the rate equation (eq 6) yields eq 7, where *k* is an apparent rate constant that incorporates a (unknown) dependence on $[BnOH]_0$. An excellent nonlinear fit of the kinetic data to eq 7 shown in Figure 7b ($R = 0.987$) yields $k = 2.14 \times 10^{-3}$ s^{-1} and $f = 0.025$ (2.5%). The striking agreement of the latter value with that derived from analysis of the independently determined data in Figure 6 (0.0374 M is 2.5% of the initial concentration of $[CL]_0 = 1.5$ M) strongly supports the hypothesis of catalyst deactivation by an impurity in all of the kinetics experiments. Finally, we found that the polymerization rate decreased by a factor of ~10 when d_8-THF (10 equiv relative to $[L^1Zn]_0$) was present (conditions: $[L^1Zn]_0 = 0.186$ M, $[BnOH]_0 = 0.130$ M, $[CL]_0 = 3.0$ or 5.0 M). These results are consistent with the aforementioned hypothesis of THF being an inhibitor in the polymerization reaction.

$$[L^1Zn]_{eff} = [L^1Zn]_0 - f[CL]_0' \quad (5)$$

$$R_p = k[L^1Zn]_{eff}[CL]_0' \quad (6)$$

$$R_p = k[L^1Zn]_0[CL]_0' - kf[CL]_0'^2 \quad (7)$$

To assess the order of the polymerization reaction with respect to BnOH initiator, kinetic experiments were performed using $[L^1Zn]_0 = 0.186$ M, $[CL]_0 = 1.5$ M, and $[BnOH]_0$ values between 0.01 and 0.5 M. The resulting plot of R_p versus $[BnOH]_0$ (Figure 8) shows that at low $[BnOH]_0$ ($\leq$0.20 M) the rate increases with increasing initiator concentration but at higher $[BnOH]_0$ (>0.20 M) the rate slows. Decomposition of the catalytic species (via ligand loss?) or Zn deactivation (via BnOH binding) may be

(26) At values of $[CL]_0 > 5$ M catalyst precipation was observed and, due to the lack of solution homogeneity under these conditions, kinetic data were not collected.

(27) Odian, G. *Principles of Polymerization*, 3rd ed.; John Wiley & Sons: New York, 1991; pp 550−551.

(28) Save, M.; Schappacher, M.; Soum, A. *Macromol. Chem. Phys.* **2002**, *203*, 889−899.

(29) Doubling $[LZn]_0$ or halving $[BnOH]_0$ changes the slopes of plots of R_p versus $[CL]_0$ but does not result in a significant change in the *x*-intercept (data not shown).

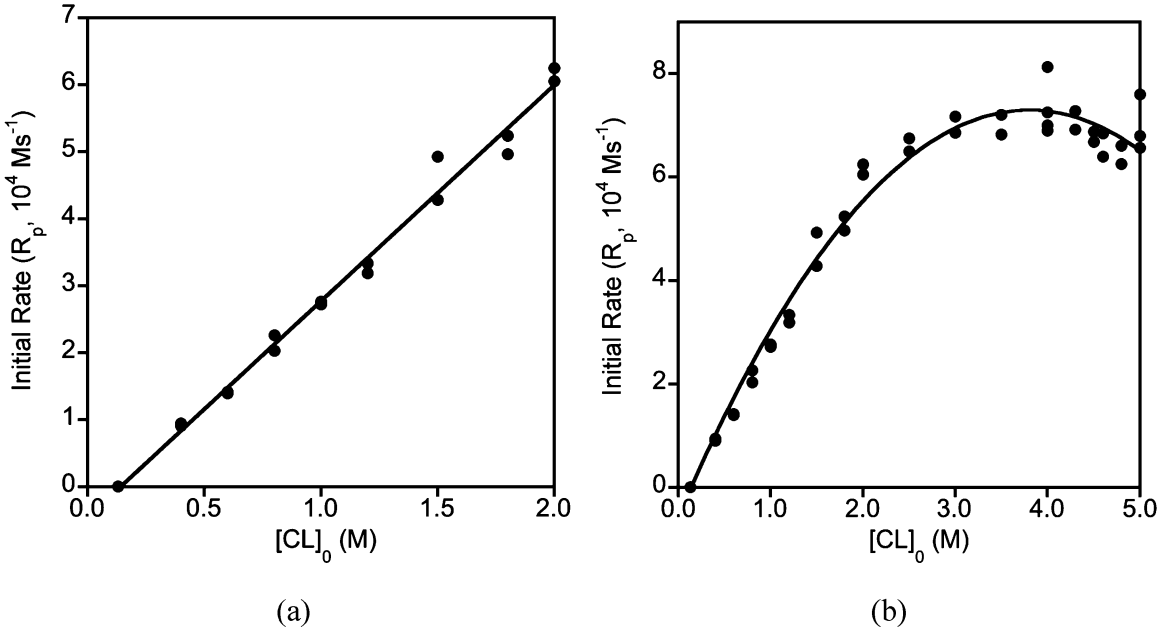

Figure 7. Plots of the initial rate of polymerization of CL vs the initial concentration of CL. Conditions: $[L^1Zn]_0 = 0.186$ M, $[BnOH]_0 = 0.13$ M, CD_2Cl_2, 25 °C. Only the data for $[CL]_0 \leq 2.0$ M are shown in (a) with a linear fit that is characterized by slope = 3.22 s^{-1}, *x*-intercept = 0.139 M, and $R = 0.994$. All of the data up to $[CL]_0 = 5.0$ M are shown in (b) with a nonlinear fit to eq 7 shown (see text for details).

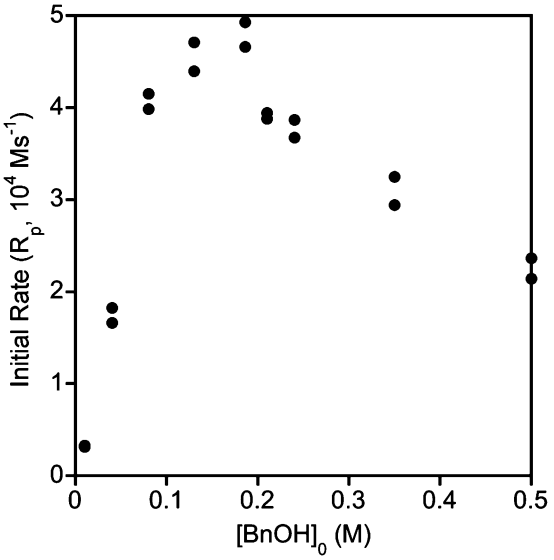

Figure 8. Plot of the initial rate of polymerization of CL vs the initial concentration of BnOH. Conditions: $[L^1Zn]_0 = 0.186$ M, $[CL]_0 = 1.5$ M, CD_2Cl_2, 25 °C.

occurring at $[BnOH]_0 > 0.20$ M, with the latter being consistent with the K_{eq} values for the aforementioned dimer/monomer equilibrium in the presense of BnOH or CL.

A general catalytic mechanism that is consistent with the kinetic data and the observed equilibria between dimeric and monomeric forms of the catalyst is shown in Scheme 3. The equilibria involving **A** ⇄ **B** and **A** ⇄ **C** have been directly observed, but the nature of **D** and the equilibria involving **B** ⇄ **C, B** ⇄ **D**, and **C** ⇄ **D** can only be inferred. The fact that R_p depends on [LZn], [CL], and [BnOH] is accounted for by the monomer-activated pathway involving complex equilibria like those shown. At this stage, further support of this mechanism remains difficult to discern with the available experimental information.

Scheme 3

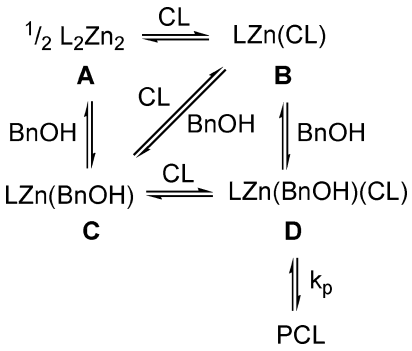

Conclusion

This work describes the combined structural, catalytic, and kinetic investigation of two sterically hindered Zn(II) bis(phenolato)amine complexes **3** and **4**. Compounds **3** and **4** adopt dinuclear structures in the solid state with a distorted tetrahedral environment about each Zn(II) ion. While the room temperature ^1H NMR spectra of **3** and **4** in CD_2Cl_2 supported the dinuclear structures observed by X-ray diffraction, cleavage to form two monomeric entities (L^1Zn) was observed upon addition of d_8-THF, BnOH, or CL. The $^1H-^1H$ NOESY NMR spectrum of **3** in a CD_2Cl_2/d_8-THF cosolvent mixture revealed chemical exchange processes consistent with interconversion of bridging and terminal phenolate arms within the dimer as well as a monomer−dimer equilibrium. The nuclearity of the species observed upon addition of d_8-THF to a CD_2Cl_2 solution of **3** was further verified through PGSE NMR experiments. The agreement between the experimental values for the diffusion coefficient and the hydrodynamic radius obtained by PGSE NMR and those estimated from the X-ray diffraction data support cleavage of dinuclear **3** into two solvated mononuclear species ($L^1Zn(d_8$-THF)). Equilibrium constants were

determined for this and related equilibria established when **3** was treated with CL or BnOH.

Both complexes **3** and **4** are effective for the controlled catalytic polymerization of CL in the presence of BnOH. Kinetic analysis of the CL polymerization by **3** in the presence of BnOH indicates a first-order dependence of the rate of polymerization on the concentration of L^1Zn and the deactivation of a fraction of **3** by a fortuitous impurity present in the system. Also, THF inhibits the polymerization of CL by complex **3,** and there is a complicated dependence of the polymerization rate on the BnOH concentration suggestive of a related inhibition process. Overall, the data support a monomer-activated mechanism for the polymerization of CL that involves equilibria among various monomeric forms of $L^1Zn(S)$ (S = THF, BnOH, and CL).

Acknowledgment. This work was supported in part by the MRSEC Program of the National Science Foundation under Award Number DMR-0212302, in part by the Petroleum Research Foundation of the American Chemical Society (45891-AC7), and in part by the University of Minnesota.

Supporting Information Available: X-ray structure of **4,** SEC traces of isolated PCL produced from **3**, CIFs, and kinetic data from Figure 7b replotted. This material is available free of charge via the Internet at http://pubs.acs.org.

IC700581S